

Experimental Study on the Effect of Attachments on the Vortex-Induced Vibration of a Centrally Slotted Box Deck

D. Xia^{1,2}, L. Dai^{2†} and L. Lin¹

¹ Fujian Provincial Key Laboratory of Wind Disaster and Wind Engineering, Xiamen University of Technology, Xiamen, Fujian, 361024, China

² University of Regina, Regina, Saskatchewan, S4S 0A2, Canada

†Corresponding Author Email: limingdai@uregina.ca

(Received October 24, 2022; accepted February 26, 2023)

ABSTRACT

Centrally slotted box decks have been commonly used as components of bridges, especially for long-span bridges. A wind tunnel experiment was conducted to investigate the effect of attachments on the vortex-induced vibration (VIV) of the deck. In this research, the characteristics of VIV responses at different attack wind angles of 5 models considering naked bridge decks, crash barriers, wind barriers, and vehicles on bridges were studied and discussed. The effects of crash barriers, wind barriers and vehicles on the VIV behaviors of the bridge deck were also investigated experimentally. Multiple lock-in wind speed intervals were found to occur for all the models considered, and the vibrating amplitude and frequency show differences in different models. The results of the study showed that, owing to the installation of crash barriers or wind barriers, the vibrating frequency at the second lock-in interval indicated a double natural frequency. However, for the naked bridge deck model, the vibrating frequencies were close to the vertical natural frequency at all lock-in regions. Additionally, the frequency showed an evolutionary characteristic from the first lock-in interval to the second lock-in interval. Generally, the installation of crash barriers and wind barriers caused an increase of 89.8% and 123.7% on maximum vibrating amplitudes respectively. The vehicles had amplification effects on the amplitudes in both lock-in regions, with an increase of 41.5% at the maximum amplitudes. This study provides a guideline for designing bridges consisting of centrally slotted box-type decks.

Keywords: Lock-in regions; Wind tunnel test; Vertical amplitude; Frequency response; Traffic flow.

NOMENCLATURE

ABS	Acrylonitrile Butadiene Styrene	VIF	Vortex Induced Force
FFT	Fast Fourier Transformation	VIV	Vortex Induced Vibration
f	frequency	y	Vertical amplitude
PIV	Particle Image Velocimetry	α	attack angle
RMS	Root Mean Square	ζ	damping ratio

1. INTRODUCTION

With the increasing flexibility and wind sensitivity of large span bridges, wind load has become one of the most important aspects in the design and usage of bridges. Among all wind-induced vibrations, VIV caused by vortex shedding has been considered a frequently occurring and serious aerodynamic phenomenon (Owen *et al.* 1996; Li *et al.* 2018; Ge *et al.* 2022). The large self-limiting vibrating amplitude may cause discomfort to the drivers or fatigue of the bridge structures (Ehsan and Scanlan 1990; Zhu *et al.* 2017); therefore, it is important to study the

VIV behavior of bridge structures for the suppression of VIV in engineering applications.

In recent decades, VIV behaviors have been experimentally and numerically studied by numerous researchers. For example, Shiraishi and Matsumoto (Shiraishi and Matsumoto 1983) classified the VIV response characteristics into three groups based on the relationship between the reduced velocity and slenderness ratio. The wind tunnel test has been proven to be a direct and effective way to investigate the VIV characteristics of long-span bridges. Based on the analysis of wind tunnel experimental data, mathematical models

were proposed to explain VIV behavior, such as Scanlan's empirical nonlinear model (Ehsan and Scanlan 1990; Simiu and Scanlan 1996) or some further modifications (Larsen 1995). Based on wind tunnel data from different types of bridge deck, Zhu *et al.* (2013) proposed a nonlinear model for vertical vortex-induced forces (VIVs) and then modified it (Zhu *et al.* 2017) by adding different nonlinear components predict stable amplitudes of VIVs.

With the development of flow visualization technology, wind tunnel tests with wind pressure recorded are also applied to show the mechanism of wind flow (Amiri *et al.* 2019; Rajasekarababu and Vinayagamurthy 2019). Liu and Zhao (Liu *et al.* 2021) investigated the nonlinear evolutionary characteristic of aerodynamic force with a synchronous pressure and vibration measurement system, interpreting the mechanism of more serious vibration for a considered central-slotted box deck, which is a type of bridge deck similar to our research. Yuan *et al.* (2017) investigated the processes of VIV for both static and dynamic models to show the contribution of the central gap of the bridge deck on the changing vortex field around the model. Xu *et al.* (2018) investigated the VIV of bridge decks by considering additional aeroelastic effect under different mass-damping conditions, which may reduce the uncertainty in prediction of the VIV performance. To evaluate the VIV amplitude of a box girder, Noguchi *et al.* (2020) applied flutter derivatives based on forced oscillation method, with verification by wind tunnel test data.

Moreover, except for the vibration amplitudes, wind speeds at which VIVs occur are also important during the service of bridges. Therefore, researches on VIV countermeasures including aerodynamic and mechanical countermeasures are investigated in existing references (Chen *et al.* 2013). In real engineering applications, attachments such as crash barriers, wind barriers, and maintenance rails are usually installed on bridges for different functions. However, the attachments installed may change the aerodynamic shape of the bridge deck and consequently change the air flow around the main girder (Zhou *et al.* 2015). Some attachments have positive effects on the suppression of VIV behavior and are therefore considered aerodynamic countermeasures, while some attachments may cause adverse effects (Bai *et al.* 2020; Yang *et al.* 2021a). Therefore, it is of great importance to investigate the effect of attachment on the aerodynamic vibration of bridges, especially for VIV behaviors, which has been commonly seen in long-span bridges (Frandsen 2001; Fujino and Yoshida 2002; Zhao *et al.* 2022). Avila (2016) conducted a wind tunnel test with the utilization of particle image velocimetry (PIV) technology to characterize the influence of a couple of solid wind barriers on the flow properties. The effect of such equipment on VIV responses was also reported by Bruno and Mancini (2002) and Xu *et al.* (2014), who concluded that it will increase the overall degree of bluffness, especially for streamlined bridge decks. Based on both experimental and

numerical methods, Zhang *et al.* (2020) analyzed the flow pattern and vortex structure around a two-box edge girder, showing that mini-triangular wind fairing can considerably suppress VIVs at different attack angles. Laima *et al.* (2018) took a twin-box girder as a section model and systematically studied the effect of handrails, crash barriers, wind barriers, maintenance rails and full ancillaries. The results show that handrails and crash barriers have a weak influence, while wind barriers and maintenance rails lead to larger pressure fluctuations. Other types of models, such as the "π" section (Bai *et al.* 2021), split three-box girder (Yang *et al.* 2021b), and asymmetrical composite beam (Wang *et al.* 2019), are also considered to show the effect of attachments on VIVs.

Centrally slotted box decks have recently become increasingly popular in large-span bridges. The VIVs of such bridge decks are found to be more serious (Liu *et al.* 2021). The suppression of vibrations is therefore necessary and important for such a bridge deck. However, even though the vibrating amplitude and frequency are discussed, few studies on the effect of attachments on VIVs of such a bridge deck are conducted in the literature. In this research, a wind tunnel test of a centrally slotted box bridge deck model was performed to investigate the effect of attachments on the VIV of the bridge. Three attack wind angles (0° , $+3^\circ$, -3°) were considered. The influences of crash barriers, wind barriers, and vehicles on both responses and frequencies were investigated and compared. The corresponding results are important in the VIV suppression design in engineering applications.

2. SECTION MODEL AND EXPERIMENTAL SETUP

The section model was based on a real suspension bridge located in Fuzhou in China, which is also a steel box girder bridge with a main span length of 719 m. The main girder of the bridge is 54.25m in width and 3.5m in depth. According to the dynamic calculation of the whole bridge, the vertical natural frequency was 0.27. The equivalent mass and mass moment were $3.015 \times 10^4 \text{ kg/m}$ and $7.515 \times 10^6 \text{ kg} \cdot \text{m}^2/\text{m}$ respectively. Figure 1 illustrates the configuration of the bridge deck of the considered suspension bridge.

The section model wind tunnel test was conducted under smooth flows at the high-speed test section of the wind tunnel lab at Xiamen University of

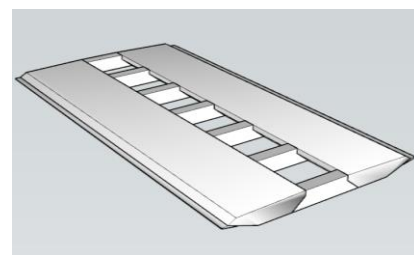


Fig. 1. Configuration of bridge deck (Xia *et al.* 2022).

Table 1 Parameters of the section model.

Parameters	unit	ratio	Prototype	model
Length	<i>m</i>	1:50	-	2.5
Width	<i>m</i>	1:50	54.25	1.085
Height	<i>m</i>	1:50	3.5	0.07
Mass	<i>kg/m</i>	1:50 ²	3.015E+04	12.06
Mass moment	<i>kg*m²/m</i>	1:50 ⁴	7.515E+06	1.2024
Vertical frequency	Hz	10.85:1	0.27	2.93



Fig. 2. Section model in wind tunnel lab.

Technology. The high-speed test section had a size of 8.0m (length) × 2.6m (width) × 2.8m (height). The wind speed at this section can be continuously adjusted from 2 m/s to 85 m/s. Both the recorded wind speed and vibration of the section model were conducted in the high-speed section. Considering the lab section size, ratio of length to width of the section model, blocking rate, scaled mass and mass moment, and the geometrical scale ratio was set as 1:50 to meet the geometrical similarity and dynamic similarity according to the [Guidelines for Wind Tunnel Testing of Bridge \(2018\)](#). Blockage of the wind tunnel test was calculated as 2.6%, which was less than 5%, indicating that no size correction was needed in this experiment according to the Design Manual for Roads and Bridges ([Highway Agency of England, 2001](#)). To ensure the scaled mass, stiffness, and mass moment, the section model was made of 3 mm thick high-quality wood. Two aluminum core beams were installed to ensure the rigidity of the model. The attachments, such as crash barriers and wind barriers, were manufactured using plastic materials (ABS).

The laser displacement meters and accelerometers are installed at the four sides of the section model (as shown in Fig. 3) to measure the instantaneous vibration amplitude and acceleration of the model respectively. For the laser displacement meter, the measure range is ±100mm, with the repeatability of 0.5um. The sensitivity of accelerometers applied is larger than 5pc/g and the sampling frequency can vary from 1Hz to 18 KHz. In the described experiment, the sampling frequencies of both laser displacement meter and accelerometer are selected as 1000Hz. The data acquisition system applied is DH5922D vibration testing system provided by Donghua Test Co., Ltd with 32-channel signal input

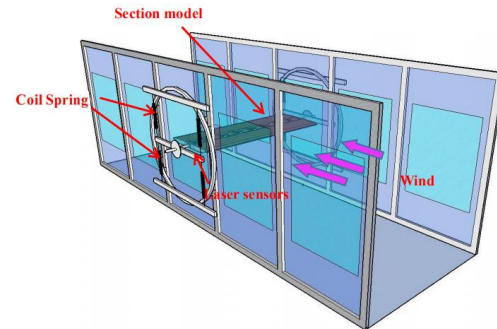


Fig. 3. Sketch of installation of model and measure system.

integrated strain conditioning. All the vibration data can be transmitted to computer for storage in real time. The inflow is controlled by setting the motor speed, and the corresponding actual wind speed is measured by a Cobra anemometer, which can report the mean speed and turbulence intensity of the income flow. Based on this, the wind speed and vibration displacement and acceleration under pre wind speed can be obtained synchronously. In this test, vibration data of duration of 60s containing 60000 data points at each wind speed are recorded.

The test setup was specially designed to conduct the wind tunnel test, and the measurement system was mounted on the outside walls of the wind tunnel. Eight linear springs were suspended to support the section model in the wind tunnel lab, enabling the vertical and torsion vibrations of the model. Four laser displacement meters and four accelerometers were arranged outside the lab to measure the dynamic response of the model, with two for each side of the lab. The displacement between the two lasers was 1194 mm. The main parameters, including mass, inertia, and frequency, are listed in Table 1. A sketch of the whole measurement system and section model is presented in Fig. 2, and the installation of the model in the wind tunnel lab is indicated in Fig. 3. As shown in Fig. 1 and Fig. 2, the investigated section model was a centrally slotted box deck with a central open space of 23.5cm at each 25.6cm along the longitudinal axis of the section model. Figure 4 shows the vibration under vertical force in still air of the section model, indicating a calculated damping ratio of 0.3% and frequency of 2.93Hz. The torsional frequency of the model can also be measured by applying torsional force in still air in this experiment. With the expression of Reynolds as $Re = \rho UL / \mu$, the scale of Reynolds number is 1:230, according to the existing research on Reynolds number effect, for section test

Table 2 Testing cases of VIV performance

Test models	Description	Damping ratio (ζ)	Attack angle (α)	Vertical Frequency
Model A	Bridge deck only	0.3%	0°, +3°, -3°	2.93 Hz
Model B	Bridge deck with crash barriers	0.3%	0°, +3°, -3°	2.87 Hz
Model C	Bridge deck with wind barriers	0.3%	0°, +3°, -3°	2.88 Hz
Model D	Bridge deck with sparse traffic flow	0.3%	0°, +3°, -3°	2.74 Hz
Model E	Bridge deck with busy traffic flow	0.3%	0°, +3°, -3°	2.75 Hz

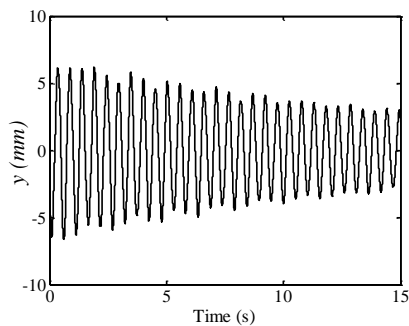


Fig. 4. Vibration of the section model in still air.

on bridge deck with sharp edges and corners, the Reynolds number effect can be neglected in wind tunnel lab unless the Reynolds number scale is larger than 1:1000 (Li 2003). Therefore, in this test, Reynolds number effect is not considered.

To distinguish different VIV behaviors under different conditions, the wind tunnel test was divided into 5 test cases, as shown in Table 2. Model A tests the VIV behavior of the considered centrally slotted box deck. Model B and Model C investigate the influence of crash barrier wind barriers on the VIV behavior of the bridge deck. Model D and Model E considered the traffic flow in real engineering applications. It should be mentioned that in real bridges, crash barriers are always installed on the bridge; therefore, for Model D and Model E, when considering traffic flow, crash barriers were installed as well. All the attachments were removable in the test.

In the wind tunnel test, the inflow velocity ranged from 1 m/s-15 m/s. The turbulence intensity was less than 1%, and the influence can be ignored. Vibrations were recorded at each approximately 0.15 m/s controlled by the motor speed of the wind tunnel. A cobra with a sampling frequency of 1000 Hz was applied to obtain the real-time wind speed and turbulence intensity, as shown in Fig. 2. To fully understand the vibration behavior, a 60s sampling time was set up for the records.

3. TEST RESULTS AND DISCUSSIONS

3.1 VIV of Bridge Deck

As indicated in Table 1, the natural vertical frequency of the model is 2.93 Hz. The vertical damping ratio was 0.30%. Three wind angles of 0°,

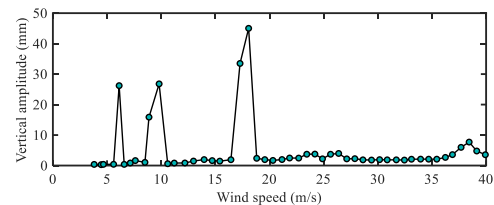


Fig. 5. VIV response of the section model vs. wind velocity for Model A.

+3° and -3° were considered in this test. Figure 5 shows the responses of the section model vs. wind speed during all stages of the VIV, including vertical VIV and torsional VIV, when the attack angle was 0°. To ensure the accuracy of recorded data, the back environment noises without income wind are recorded first; RMS (root mean square) of noises (without income flow) and RMS of displacement under income flow are compared as:

$$error = 1 - \frac{RMS_{wind} - RMS_{noise}}{RMS_{wind}} \quad (1)$$

In the equation, RMS_{wind} is the root mean square of recorded displacements with income wind, RMS_{noise} is the root mean square of recorded displacements without income wind which can reflect the environment noise in the wind tunnel test. Based on the test result, the error calculated is 0.0004, indicating that the environment noise can be neglected in the test, ensuring the reliability of the recorded data.

In Fig. 5, the x -axis indicates the wind speed and y -axis represents the vertical amplitude as per incoming wind speed. It is worth to mention that, the amplitude and wind speed are converted to those of prototype bridge based on scaled ratios. As indicated in Fig. 5, the relationship of the wind speed and vertical amplitude for Model A was presented, considering the root mean square of the VIV displacement at a certain wind speed. For a bluff body, a regular pattern of vortices develops in the downstream region that expects periodic pressure on the body. For a certain wind velocity, the frequency of vortex shedding may approach or be very close to the natural frequency of the structures. When the ratio of the two frequencies becomes unity, the vibration of the structure takes control of the shedding frequency over the bandwidth. The phenomenon described above was usually called lock-in vibration. When the lock-in region occurs, the structural vibration will have large amplitudes, as shown in Fig. 5. It should be mentioned that during the test, 60000 data points

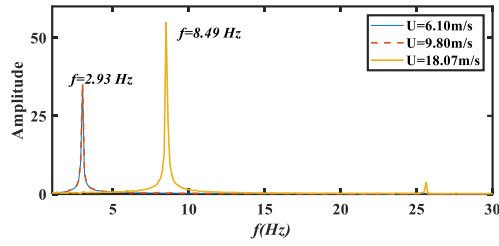
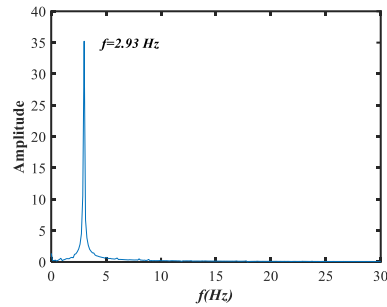
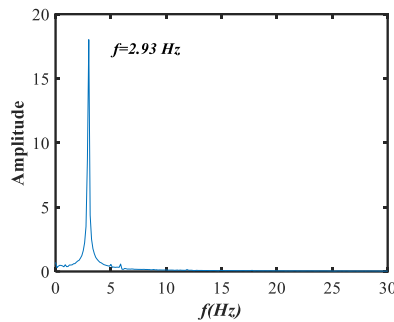


Fig. 6. FFT of the VIV displacement at different wind speeds.



(a)



(b)

Fig. 7. FFT of the vertical VIV displacement (a. first vertical lock-in region $U=6.11\text{m/s}$; b. second vertical lock-in region $U=8.90\text{m/s}$).

with duration of 60s are collected at per wind speed. To ensure the reliability of the data, data from 20s-28s with 8000 data points are used for analysis. The vertical amplitudes in the paper are RMS based on such 8000 data points.

Three lock-in regions can be recognized in the VIV vertical responses of the section model. With the application of fast Fourier transformation (FFT), the frequency responses of the displacements can be obtained in Fig. 6. With the three FFTs of maximum points, as shown in Fig. 6, one can easily distinguish the frequency of the response. Dominant 8.49 Hz is found for the third maximum points, indicating a torsional response here owing to the torsional frequency of the model was measured as 8.49 Hz. Therefore, it can be concluded that for Model A without any attachment, two vertical locks in the region and one torsional lock region can be recognized. It should be mentioned that this research mainly focuses on the vertical VIV

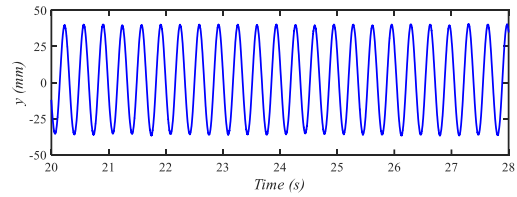


Fig. 8. Vertical time history of displacement at $U=6.11\text{m/s}$.

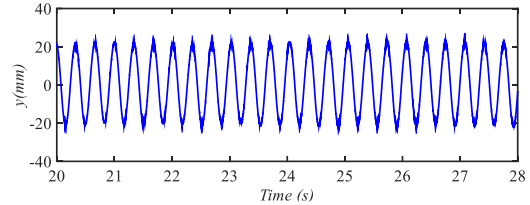


Fig. 9. Vertical time history of displacement at $U=9.80\text{m/s}$.

behaviors of the section model with different attachments. Therefore, in the following section, only the vertical VIV will be discussed.

The wind velocity at the first vertical lock-in region was $5.60\text{m/s} < U < 6.58\text{m/s}$, and $8.49\text{m/s} < U < 10.60\text{m/s}$ for the second one. The vertical maximum amplitudes at the first region (26.0mm) are slightly smaller than those at the second region (26.8mm). Fig. 6 shows the FFT of the vertical VIV displacement at two vertical regions. As illustrated in Fig.7a, at the first vertical lock-in region, the dominant frequency was $f=2.93\text{ Hz}$, which is the same as the natural frequency of the section model; however, other frequencies may occur even though with a small amplitude. In the second vertical lock-in region, the model also vibrates frequency $f=2.93\text{ Hz}$ as shown in Fig.7b. The time histories of the VIV response at the two lock-in regions are displayed in Fig. 8 and Fig. 9, respectively, in which periodic responses can be found in both figures. Therefore, for Model A with only bridge deck, the vertical VIV of the considered centrally slotted box deck will suffer two lock-in regions with the same dominant frequency.

The above description is based on a wind attack angle of 0° . In the wind tunnel test, three wind attack angles were considered. Figure 10 shows a comparison of the vertical VIV response of the section model based on three attack angles. It is worth to point that only vertical response and vertical VIV are discussed in the following sections. As shown in the figure, the VIV responses are very different when comparing the three attack angles. The lock in regions has been changed by comparing a 0° attack angle. When considering the lock-in region, only the vertical lock-in region can be found for -3° , but it has the maximum response among all the angles. The lock-in region for $+3^\circ$ was $6.76\text{m/s} < U < 8.22\text{m/s}$ and $9.90\text{m/s} < U < 10.79\text{m/s}$, and both lock-in regions were shifted to the right sides. When the angle was changed to -3° , one lock-in region vanishes, and the lock-in wind speed was changed to $6.43\text{m/s} < U < 7.83\text{m/s}$, with maximum amplitude of 29 mm.

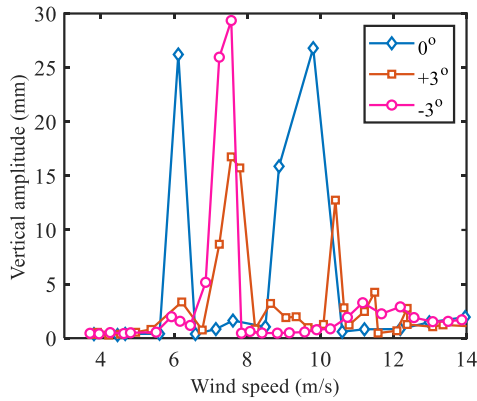


Fig. 10. Vertical VIV response of the section model vs. wind velocity based on three attack angles.

To investigate the effect of attachment on the VIV of the section model, different attachments were installed on the section model, and the vibration results are discussed below.

3.2 VIV of bridge Deck with Crash Barriers

In real engineering applications, crash barriers are often installed to prevent uncontrolled vehicles from crossing bridges. However, it is well accepted that crash barriers may affect the VIV behavior of bridges. In this experiment, two 1.5 m height crash barriers (3 cm height in the wind tunnel test) were installed on both sides of the section model. The model size can be seen in Fig. 11. Figure 12 shows the vertical VIV response of the section model with Model B. As indicated, two lock-in regions can be found for all three attack angles. Generally, the lock-in regions are shifted to the left sides which is opposite with Model A. For Model A with bridge deck only, the model is easy to be torsional as indicated in Fig.5. The attack angle may increase the ability twisting resistance; therefore the lock-in region occurs at larger wind speeds. However, with the installation of crash barriers (Model B), torsional amplitudes significantly decrease. Comparing with Model A, Model B shows a much better performance on twisting resistance of the bridge deck, therefore, the attack angle mainly affect the vertical vibration. For Model B, in the first region, the vertical amplitude with a value of 41 mm occurs when the attack angle was -3° , while the maximum amplitude with a value 61.5mm can be found in the second lock-in region. The amplitudes in the second lock-in region were



Fig. 11. Figure of bridge deck with crash barriers (Model B).

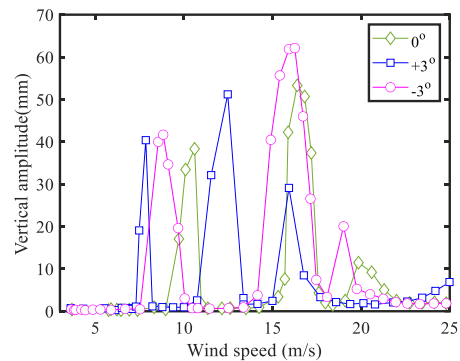


Fig. 12. Vertical VIV response of the section model vs. wind velocity based on three attack angles.

generally larger than those in the first region. Table 1 summarizes the lock-in regions at the three attack angles. From the table, for Model B, the most unfavorable case is -3° attack angle with the largest vertical amplitude and longest lock-in interval.

Except for the VIV lock-in region, this research also focuses on the vortex excited vibration evolutionary characteristics. Taking the 0° attack as an example, Fig. 13 shows the vertical VIV response of the section model vs. the wind velocity at 0° . The VIV regions were divided into five stages: pre-VIV, ascent, extreme point, descent and ending of VIV parts, as shown in Fig. 13. The maximum amplitudes were 38 mm and 50.3mm at the first and second locks in the region, respectively, as shown in Fig. 13. Additionally, from the time history in Fig. 14, the second extreme point had a higher vibration frequency than the first one. To analyze the evolutionary characteristics, the fast transform Fourier (FFT) method was applied to obtain the frequency responses of the five stages. Wind

Table 3 Wind velocity of VIV at different attack angles.

Attack angle	Wind speed (m/s)	
	First lock-in region	Second lock-in region
0°	$8.96 < U < 10.96$	$14.24 < U < 17.60$
$+3^\circ$	$7.27 < U < 8.21$	$10.73 < U < 13.35$
-3°	$7.51 < U < 10.03$	$14.18 < U < 17.50$

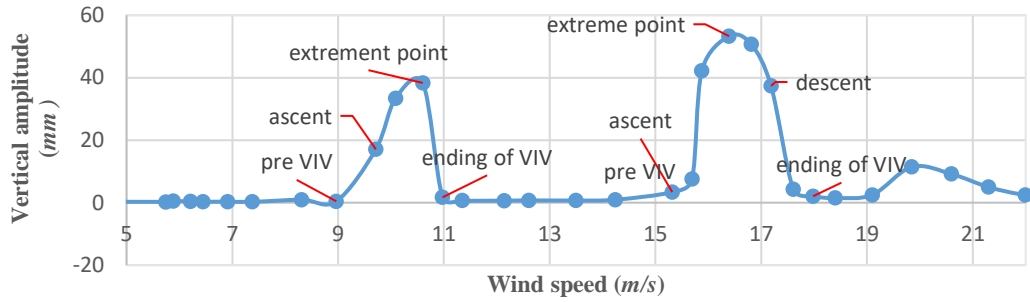


Fig. 13. Vertical VIV response of the section model vs. wind velocity at an attack angle of 0°

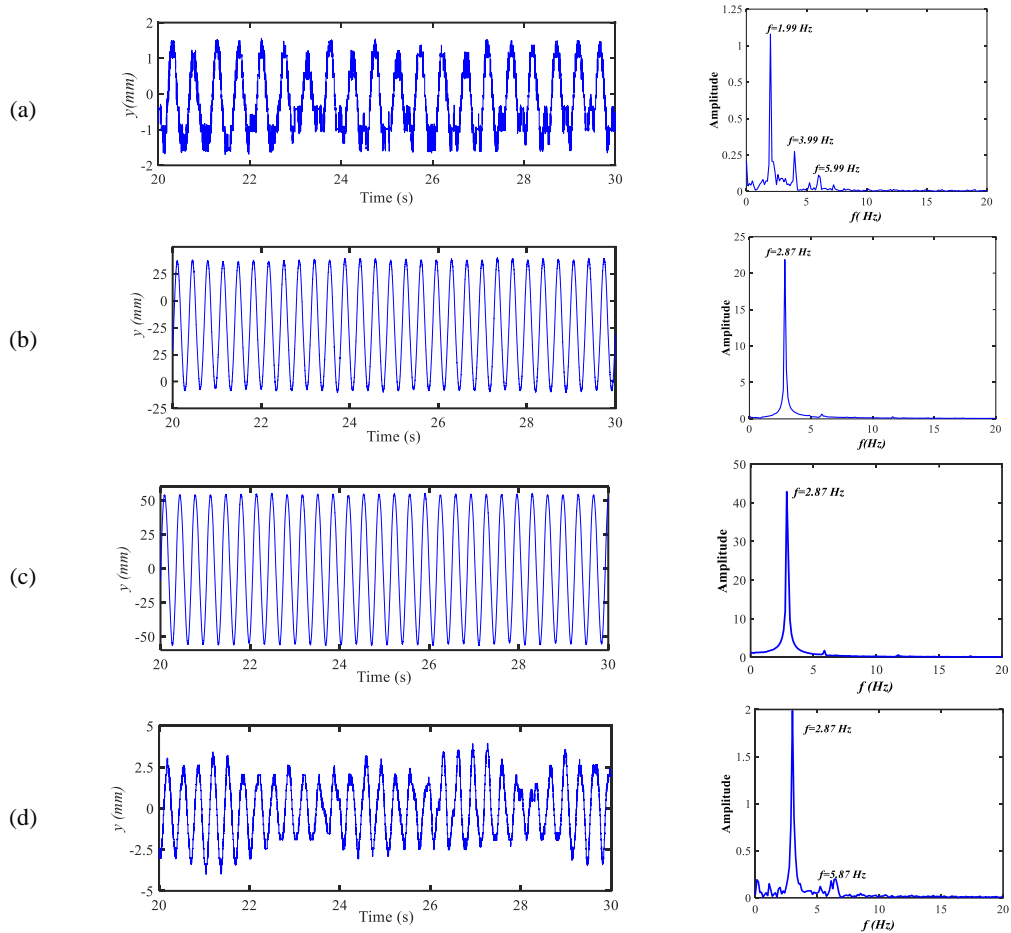


Fig. 14. Time histories and frequency responses of different stages at first region at attack angle 0° (a) pre VIV; (b) ascent; (c) extreme point; (d) ending of VIV).

velocities $U=8.96\text{m/s}$, 10.08 m/s , 10.59 m/s , and 10.96 m/s at the first lock-in region and $U=14.24\text{ m/s}$, 15.68 m/s , 16.38 m/s , 16.80 m/s , and 17.60 m/s at the second lock-in region are considered as the five stages.

As indicated in Fig. 13, in the pre-VIV stage, the amplitude of the vibration is almost zero, and in the ascent stage, the amplitude increases significantly to the extreme point. After that, the amplitude gradually decreases until the end of the VIV. Based on the FFT analysis, Fig. 14 shows the time histories and frequency responses of different stages at the first lock-in region with the first harmonic vibration. At the pre-VIV stage, the response was

highly random and fluctuating, and the system shows a multipeak vibration with three dominant frequencies. As the wind speed increased to $U=10.08\text{m/s}$ at the descent stage, a jump in the response from the small amplitude to the high amplitude limit cycle was observed with the dominant frequency $f=2.87\text{ Hz}$, which is the same as the natural frequency of Model B. When the wind speed increases to $U=10.59\text{m/s}$ at the extreme point, the natural frequency still shows dominance; however, the vibration amplitude reaches a maximum of 38.5 mm . After the extreme point, the system suddenly changes to small amplitude vibration, and the structure exhibits a weakly

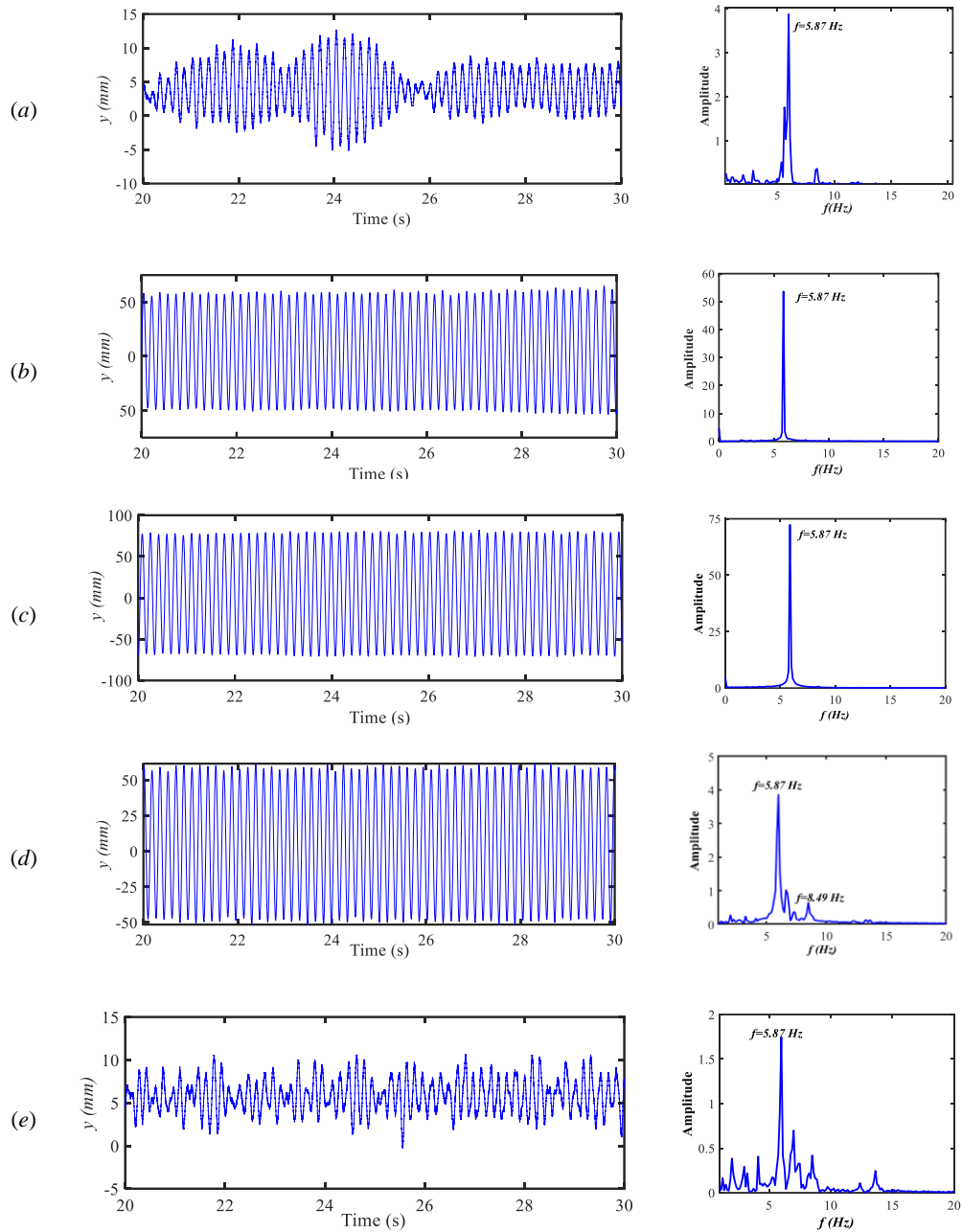


Fig. 15. Time histories and frequency responses of different stages at second region at attack angle 0° (a) pre VIV;(b) ascent; (c)extreme point;(d) descent; (e) ending of VIV.

intermittent nature, which indicates the VIV sensitivity of the model at such a wind speed. The natural frequency $f=2.87$ Hz still plays an important role in the frequency response; however, $f=5.87$ Hz, which was close to double the natural frequency of the model, also shows an ignorable part.

Figure 15 illustrates the time histories and frequency responses of different stages in the second region. Generally, from the frequency response, a second harmonic vibration with a dominant frequency $f=5.87$ Hz, which is close to double the natural frequency, can be observed in all five stages. Such a phenomenon was very different

from the vibration of Model A, in which all the vibrations in the lock-in region were dominated by the natural frequency. As shown in Fig. 15, from the pre-VIV stage to the end of VIV, the frequency $f=5.87$ Hz showed an increasing and then decreasing dominance in the response. The vibration amplitudes also had a similar tendency. Additionally, an interesting phenomenon can be seen that the frequency $f=8.49$ Hz, which was close to torsional, also shows a dominant role at the end of VIV. Figures 16 and 17 show three-dimensional frequency responses at attack angles $+3^\circ$ and -3° , respectively, indicates a similar tendency with

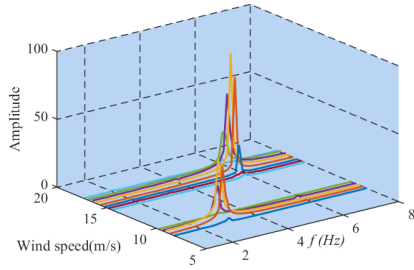


Fig. 16. Frequency response at different wind speeds in lock-in regions at a wind attack angle of +3°.

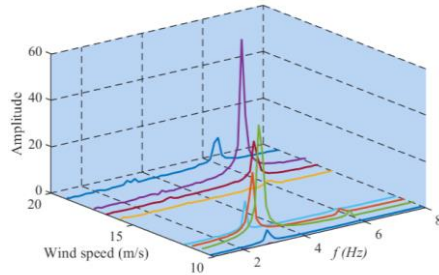


Fig. 17. Frequency response at different wind speeds in lock-in regions at a wind attack angle of -3°.

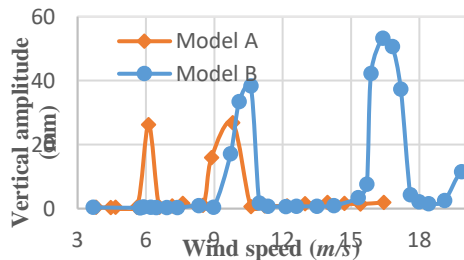


Fig. 18. Comparison of VIV responses of Model A and B at an attack angle of 0°.

attack 0°. It should be noted that from the vertical VIV response in Fig. 13, torsional VIV also occurred just after the end of VIV in the second lock-in region. This research focuses on vertical VIV, and the characteristics of torsional VIV will not be investigated in this research.

Figure 18 compares the VIV responses of Model A (bridge deck only) and Model B (with crash barriers) at an attack angle of 0°. With the installation of crash barriers, VIV responses significantly increase from a maximum value of 26.5 mm in Model A to 50.3 mm in Model B, with an increase of 89.8%. Additionally, the crash barriers have an amplification effect on the range of lock-in ranges. Lock-in wind speeds increase with the installation of crash barriers. It should be emphasized that, even though in both models, two lock-in regions can be observed during the experiment; the vibrations at the second lock-in region are totally different. As discussed above, for Model A, the natural frequency plays a dominant role in both lock-in regions; however, in Model B, $f=5.87$ Hz, which is double the fundamental frequency. This may be because compared with Model A, the crash barriers reduce the size of the vortex and increase the high frequency of vortex shedding and are consequently excited.

3.3 VIV of bridge deck with wind barriers (Model C)

For the sake of the serviceability of large-span bridges, wind barriers are often installed on both sides of bridges to reduce wind on the bridge deck and ensure the safety of vehicles. Wind barriers of 6 cm height with a 60% ventilation rate are considered in this experiment (as indicated in Fig. 19a) to show the effect on the VIV responses of the bridge deck. Fig. 19b shows the VIV responses of Model C with the installation of wind barriers under smooth oncoming flow at three attack angles. Similar to Model B, two lock-in regions can still be observed. The maximum vertical amplitude of 62.5 mm occurs when the attack angle is +3°, with a slight increase comparing Model B, which shows an agreement with result in the reference (Wang *et al.* 2019). The maximum VIV response occurred at a higher wind speed when the attack angle is 0°, with an increasing of 123.7% of maximum value comparing Model A. The VIV time histories and frequency responses of $U=9.00$ m/s at the first lock-in region and $U=16.05$ m/s at the second lock-in region are shown in Fig. 20. The time history and frequency response indicate a vibration excited by

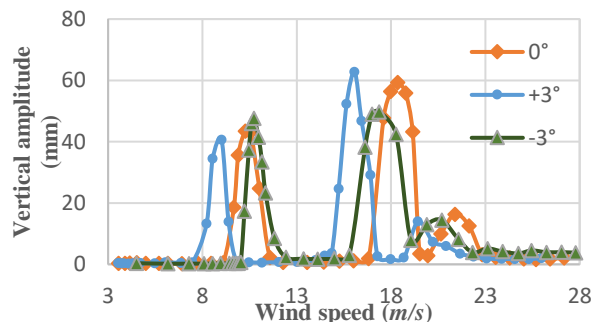


Fig. 19. Experiment of Model C with wind barriers (a) section model in wind tunnel lab; (b) VIV response of Model C at three attack angles.

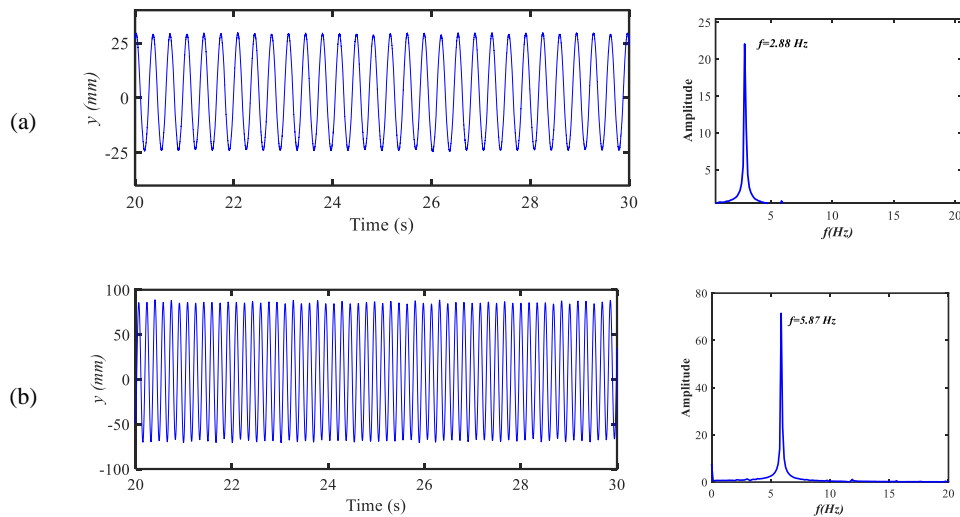


Fig. 20. Time history and frequency response of VIV at (a) $U=9.00\text{m/s}$; (b) $U=14.67\text{m/s}$.

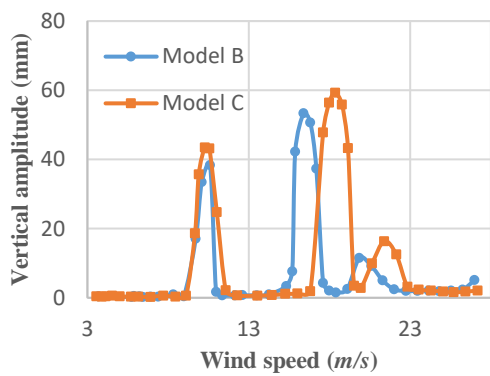


Fig. 21. Comparison of VIV responses of Model B and C at an attack angle of 0° .

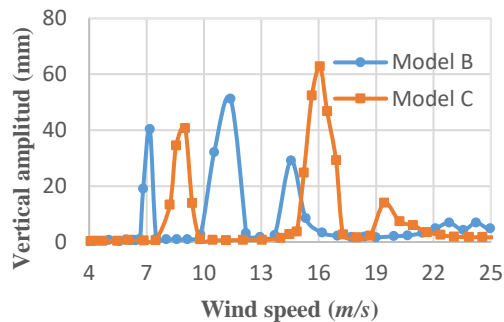


Fig. 22. Comparison of the VIV responses of Model B and C at an attack angle of $+3^\circ$.

vortex shedding at $f=2.88\text{Hz}$, which is the fundamental frequency of Model C. With the increase in wind speed, VIV excited by higher frequency vortex shedding at $f=5.87\text{ Hz}$ can be found, as shown in Fig. 20b, with the increase in amplitudes. Such a phenomenon is similar to that in Model B. Interestingly, the shape types of the crash barriers and wind barriers were similar even though the sizes are different, indicating that such an attachment type may cause vibrations excited by high vortex shedding. Comparing the VIV response

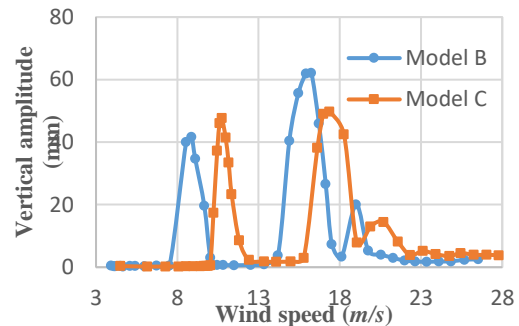


Fig. 23. Comparison of VIV responses of Model B and C at an attack angle of -3° .

of the bridge deck with crash barriers (Model B) and wind barriers (Model C), as indicated in Fig. 21, the wind barriers have an amplification effect on both vibration amplitudes and wind speeds of VIV. As indicated in Fig. 21-Fig. 23, comparisons of the VIV response at three attack angles are presented, implying that the most unfavorable attack angle was $+3^\circ$ for Model C with maximum amplitudes of 62.73 mm at $U=16.06\text{ m/s}$ and -3° for Model B with a maximum amplitude of 62.11 mm at $U=16.25\text{ m/s}$.

3.4 VIV of Bridge Deck with Sparse Traffic Flow (Model D)

It has been well accepted that VIV is sensitive to the shape of structures. In real engineering applications, vehicles also move on the bridge deck and inevitably change the wind field on the bridge deck and therefore may affect the VIV events of the structures. Investigations on the influence of vehicles on VIV behavior on bridge decks were necessary in engineering applications. In this research, to investigate the effect of vehicles, two kinds of traffic flows were considered, namely, sparse traffic flow (Model D) and busy traffic flow (Model E). It should be mentioned that crash



Fig. 24. Experimental model of Bridge deck with spares traffic flow.

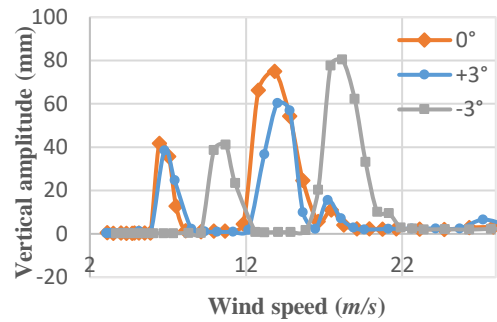


Fig. 25. Comparison of the VIV responses of Model D at an attack angle of +3°.

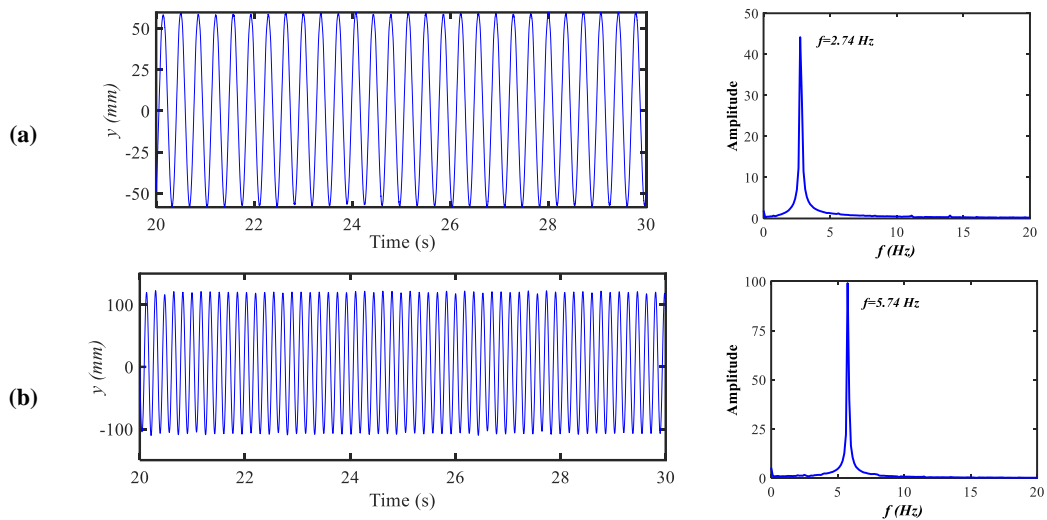


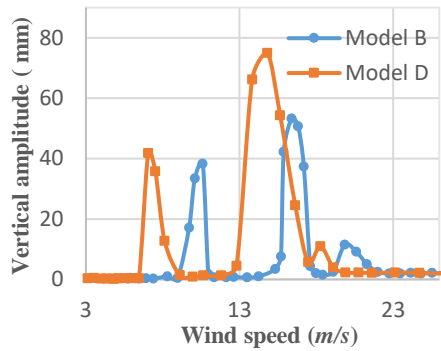
Fig. 26. Time histories and frequency response of VIVs of Model D at (a) $U=6.44\text{m/s}$; (b) $U=13.8\text{m/s}$ at wind attack angle 0°

barriers are usually installed in the use of bridges. Therefore, in this experiment, crash barriers were installed on the bridge deck to study the influence of the vehicles. Vehicles were selected as scaled 1:50 vehicle models, which have the same scale ratio as the bridge deck model. To simulate the sparse traffic flow, fewer vehicles were randomly arranged on the bridge deck, as shown in Fig. 24. To simulate the real situation, different vehicle types were selected, such as cars, buses, and trucks, as indicated in Fig. 24.

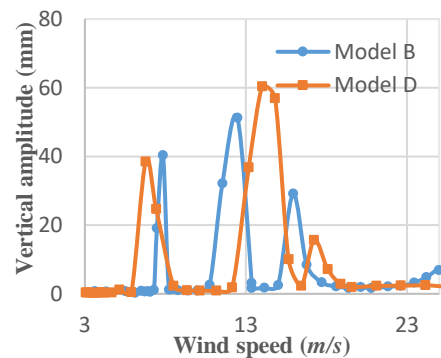
The VIV responses of the bridge deck with vehicles at three attack angles are shown in Fig. 25. As indicated, the most unfavorable attack angle is -3° , with maximum vibration amplitude of 80.44 mm, which is different from Model C. At all three attack angles, two lock-in regions can be observed for vertical VIVs. With the attack angle changing from 0° to -3° , the wind speed at the second lock-in region increases significantly. Figure 26 Selected time histories and frequency responses by the FFT method of VIVs at $U=6.44\text{m/s}$ at the first lock-in region and $U=13.8\text{m/s}$ at the second lock in the region at an attack angle of 0° . Both limited cycle vibrations can be seen at the two wind speeds with two different frequencies. It should be mentioned that with the arrangement of vehicles on the bridge deck, the fundamental frequency slightly changes as

$f=2.74\text{ Hz}$, as indicated in Table 2. In Fig. 26, VIVs are excited by vortex shedding at $f=2.74\text{ Hz}$ and $f=5.74\text{ Hz}$, which was close to double the fundamental frequency. This result is similar to the VIV responses for Model C, indicating that even though the vehicles may affect the aerodynamic shape of the bridge deck, such a model with crash barriers still has the characteristics that it will suffer VIVs at two different frequencies.

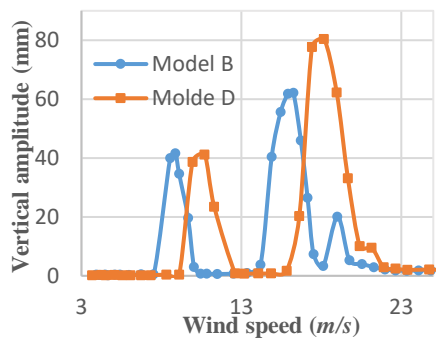
Figure 27 compares the VIV responses of Model B and Model D at three attack angles to investigate the effect of vehicles on VIVs. For all three attack angles, the vehicles have an amplification effect on the VIV amplitudes at the second lock-in regions with high-frequency VIVs, with an increase of 41.5 % if the maximum amplitude. Analogous to Model C, a wind attack angle of -3° is unfavorable among all three cases. In such a case, the vehicles exerted a significantly negative effect on the VIV of the bridge deck. The maximum vibration amplitude increases from 62.11 mm to 80.44 mm. Considering all three wind attack angles, the vehicles generally have an adverse effect on the VIVs of the bridge deck, which is different from the results in reference (Wang *et al.* 2019), in which the asymmetrical composite beam is considered. This may indicate that the shape of the cross-section may also be



(a)



(b)



(c)

Fig. 27. Comparison of the VIV responses of Model D at an attack angle; (a): 0° (b): -3° (c): +3°.

important in investigating the effect of attachments on VIVs, which is not studied in this research.

3.5 VIV of Bridge Deck with Busy Traffic Flow (Model E)

In real applications, the full arrangement of vehicles on bridge decks can be commonly seen, especially during rush hour for work. In this research, to show the influence of busy traffic flow, the vehicles were fully arranged on the bridge deck. Since there is no a certain criterion for the arrangement, the rules in *General Specification for Design of Highway Bridges and Culverts (1989)* were selected for the modeling vehicles of the experiments. Figure 28 indicates Model E in the wind tunnel lab. The VIV responses in Models B, D and E are compared in Fig. 29 and Fig. 30, indicating that both the sparse



Fig. 28. Experimental model of Model E in wind tunnel lab.

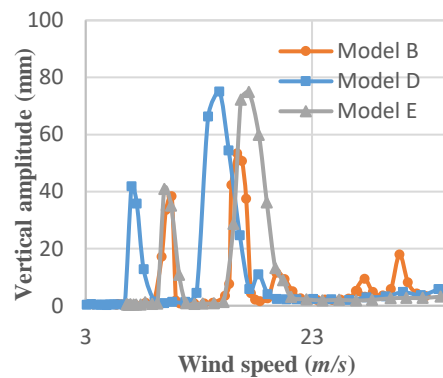


Fig. 29. Comparison of the VIV response between different models at an attack angle of 0°.

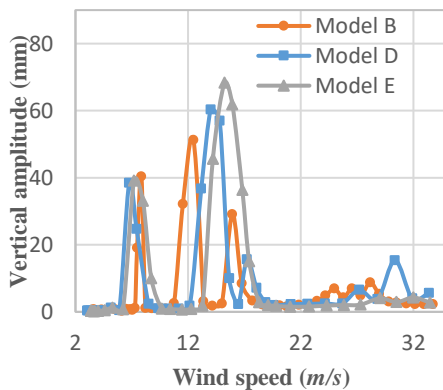


Fig. 30. Comparison of the VIV response between different models at an attack angle of +3°.

and busy traffic flows increase the VIV responses compared to Model B without traffic flow at both lock-in intervals. However, compared with sparse traffic flow, the increase in vehicles will have a slight change in amplitudes of VIV responses but changes lock-in wind speeds for both lock-in intervals.

Figures 31-Fig. 32 compare the VIV responses at three attack angles of Model D and Model E, respectively. For Model D with sparse traffic flow, the VIVs are more sensitive to the attack angles. For Model E with more vehicles on bridge deck, the VIV responses have slight variation even though

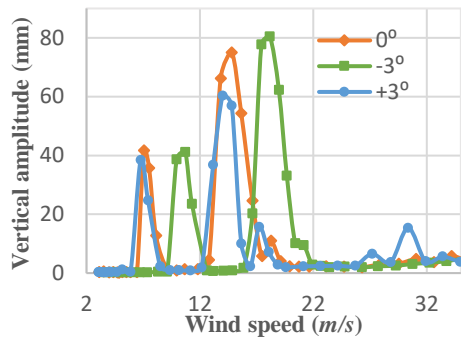


Fig. 31 Comparison of the VIV response of Model D at different attack angles.

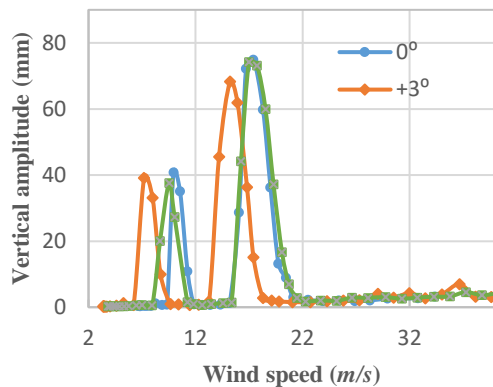


Fig. 32. Comparison of the VIV response of Model E at different attack angles.

wind speeds at lock-in regions are changed. Generally, the traffic flows have an amplification effect on the VIV response for the considered centrally slotted box bridge deck, which shows a difference from the results in references (Wang *et al.* 2019), indicating that the effect of vehicles on VIVs should take the bridge deck type into consideration.

4. CONCLUSIONS

In this research, the influences of crash barriers, wind barriers and traffic flows on the aerodynamic response of a centrally slotted box bridge deck were investigated based on a wind tunnel test. On the basis of the analysis, the following conclusions were obtained:

- (1) For the centrally slotted box bridge deck considered in this test, two vertical lock-in regions can be identified with the same vibration frequency in the two lock-in regions.
- (2) With the installation of crash barriers, the vibration response and lock-in wind velocity at VIVs increase significantly. However, in the second lock-in region, the system vibration is dominant at a high frequency, which is close to double the vertical natural frequency. The vibrating frequency shows an evolutionary characteristic in the lock-in

regions.

- (3) Due to the similar shape type with crash barriers, the change in dominated frequency still exists with the application of wind barriers. Compared with crash barriers and wind barriers, wind barriers have a slight effect on the amplitudes of the VIVs, which shows an agreement with results in the references.
- (4) By changing the aerodynamic shape of bridge decks, vehicles on the bridge have an adverse effect on VIVs with larger vibration amplitudes for the considered centrally slotted box deck, which is different from the results obtained in references for an asymmetrical composite beam. The arrangement of traffic flow slightly changes the VIV response but has a significant effect on wind speed in lock-in regions.
- (5) The effect of vehicles differed from the results in the references considered; indicating that the bridge deck type should be taken into consideration when investigating the influence of vehicles.
- (6) In this research, three wind attack angles were considered (0° , $+3^\circ$ and -3°). The influence of the three attack angles was weak compared with the effect of attachments on both VIV amplitudes and frequencies.

ACKNOWLEDGEMENTS

This research was funded by Natural Sciences and Engineering Research Council of Canada (NSERC), Fujian provincial project of Transportation Science and Technology (202022), the Science and Technology Project of Fujian Province (2020H6022, 2021Y0045), and Chinese Scholarship Council (CSC).

REFERENCES

- Amiri, M., M. Kahrom and A. Teymourtash (2019). Aerodynamic analysis of a three-bladed pivoted savonius wind turbine: wind tunnel testing and numerical simulation. *Journal of Applied Fluid Mechanics* 12(3), 819-829.
- Avila-Sanchez, S., O. Lopez-Garcia, A. Cuerva and J. Meseguer (2016). Characterisation of cross-flow above a railway bridge equipped with solid wind barriers. *Engineering Structures* 126, 133-146.
- Bai, H., N. Ji, G. Xu and J. Li (2020). An alternative aerodynamic mitigation measure for improving bridge flutter and vortex induced vibration (VIV) stability: Sealed traffic barrier. *Journal of Wind Engineering and Industrial Aerodynamics* 206, 104302.
- Bai, H., R. Li, G. Xu and A. Kareem (2021). Aerodynamic performance of Π -shaped composite deck cable-stayed bridges including

- VIV mitigation measures. *Journal of Wind Engineering and Industrial Aerodynamics* 208, 104451.
- Bruno, L. and G. Mancini (2002). Importance of deck details in bridge aerodynamics. *Structural Engineering International* 12 (4), 289-294.
- Chen, W., D. Xin, F. Xu, H. Li, J. Ou and H. Hu (2013). Suppression of vortex induced vibration of a circular cylinder using suction based flow control. *Journal of Fluids Structures* 42, 25-39.
- Ehsan, F. and R. H. Scanlan (1990). Vortex-induced vibrations of flexible bridges. *Journal of Engineering Mechanics* 116(6), 1392-1411.
- Frandsen, J. B. (2001). Simultaneous pressures and accelerations measured full-scale on the Great Belt East suspension bridge. *Journal of Wind Engineering and Industrial Aerodynamics* 89 (1), 95-129.
- Fujino, Y. and Y. Yoshida (2002). Wind-induced vibration and control of Trans-Tokyo Bay crossing bridge. *Journal of Structural Engineering* 128 (8), 1012-1025.
- Ge, B., R. Ma, F. Li, X. Hu, and A. Chen (2022). Probabilistic vortex-induced vibration occurrence prediction of the twin-box girder for long-span cable-stayed bridges based on wind tunnel test. *Engineering Structures* 262, 114325.
- Guidelines for Wind Tunnel Testing of Bridges* (2018) China Communication Press, Beijing, China.
- Highway Agency of England* (2001). Design Manual for Roads and Bridges (Part 3) Design Rules for Aerodynamic Effects on Bridges. Report No. BD 49/01. Highway Agency of England, UK.
- Highway Planning and Design Institute of the Ministry of Transportation* (1989). General specification for design of highway bridges and culverts, JTJ 021-89, Beijing, China.
- Laima, S., H. Li, W. Chen and J. Ou (2018). Effects of attachments on aerodynamic characteristics and vortex-induced vibration of twin-box girder. *Journal of Fluids and Structures* 77, 115-133.
- Larsen, A. (1995). A generalized model for assessment of vortex-induced vibrations of flexible structures. *Journal of Wind Engineering and Industrial Aerodynamics* 57 (2-3), 281-94.
- Li, J. (2003). *Research and Control on Reynolds Number Effect of Bridge Section*, Ph.D. thesis, Tongji University, Shanghai, China.
- Li, M, Y. Sun, H. Jing and M. Li (2018). Vortex-induced vibration optimization of streamline box girder by wind tunnel test. *KSCE Journal of Civil Engineering* 22(12), 5143-53.
- Liu, S., L. Zhao, G. Fang, C. Hu and Y. Ge (2021). Investigation on aerodynamic force nonlinear evolution for central-slotted box girder under torsional vortex-induced vibration. *Journal of Fluids and Structures* 106, 103380
- Noguchi, K., Y. Ito and T. Yagi (2020) Numerical evaluation of vortex-induced vibration amplitude of a box girder bridge using forced oscillation method. *Journal of Wind Engineering and Industrial Aerodynamics* 196, 104029.
- Owen, J., A. Vann, J. Davies and A. Blakeborough (1996). The prototype testing of Kessock Bridge: response to vortex shedding. *Journal of Wind Engineering and Industrial Aerodynamics* 60, 91-108.
- Rajasekarababu, K. and G. Vinayagamurthy (2019). Experimental and Computational Simulation of an Open Terrain Wind Flow around a Setback Building using Hybrid Turbulence Models. *Journal of Applied Fluid Mechanics* 12(1), 145-154.
- Shiraishi, N. and M. Matsumoto (1983). On classification of vortex-induced oscillation and its application for bridge structure. *Journal of Wind Engineering and Industrial Aerodynamic* 14, 419-30.
- Simiu, E. and R. H. Scanlan (1996). *Wind Effects on Structures: Fundamentals and Applications to Design*, 3rd Ed. John Wiley & Sons, New York, USA.
- Wang, J., C. Ma, M. Li, N. Yeung and S. Li (2019). Experimental and numerical studies of the vortex-induced vibration behavior of an asymmetrical composite beam. *Advances in Structural Engineering*.
- Xia, D., L. Dai and L. Lin (2022). Identification of the Nonlinear Aerodynamic Load of vortex-induced vibration for a centrally slotted box deck model based on a wind tunnel test. *Journal of Vibration Engineering and Technologies*.
- Xu, K., Y. Ge, L. Zhao and X. Du (2018). Calculating vortex-induced vibration of bridge decks at different mass-damping conditions. *Journal of Bridge Engineering* 23(3), 04017149.
- Xu, F., B. Li, S. Cai and Z. Zhang (2014). Experimental investigations on aerostatic characteristics of bridge decks under various conditions. *Journal of Bridge Engineering* 19 (7), 27-35.
- Yang, F., S. Zheng, Q. Zhou, Z. Yan, Z. Ding and X. Tai (2021a). Vortex-excited force evolutionary characteristics of split three-box girder bridges during vortex-induced vibration. *Journal of Wind Engineering and Industrial Aerodynamics* 218, 104762.
- Yang, Y., S. Kim, Y. Hwang and H. Kim (2021b). Experimental study on suppression of vortex-

- induced vibration of bridge deck using vertical stabilizer plates. *Journal of Wind Engineering and Industrial Aerodynamic* 210, 104512.
- Yuan, W., S. Laima, W. Chen, H. Li and H. Hu (2017). Investigation on the vortex-and-wake-induced vibration of a separated-box bridge girder. *Journal of Fluids and structures* 70, 145-161.
- Zhang, T., Y. Sun, M. Li and X. Yang (2020). Experimental and numerical studies on the vortex-induced vibration of two-box edge girder for cable-stayed bridges. *Journal of Wind Engineering and Industrial Aerodynamics* 206, 104336.
- Zhao, L., W. Cui, X. Shen, S. Xu, Y. Ding and Y. Ge (2022). A fast on-site measure-analyze-suppress response to control vortex-induced-vibration of a long-span bridge. *Structures* 35, 192-201.
- Zhou, Z., T. Yang, Q. Ding and Y. Ge (2015). Mechanism on suppression in vortex-induced vibration of bridge deck with long projecting slab with countermeasures. *Wind and Structures: An International Journal* 20(5), 643-660.
- Zhu, L., X. Meng and Z. Guo (2013). Nonlinear mathematical model of vortex-induced vertical force on a flat closed-box bridge deck. *Journal of Wind Engineering and Industrial Aerodynamics* 122, 69-82.
- Zhu, L., X. Meng, L. Du and M. Ding (2017). A simplified nonlinear model of vertical-induced force in box decks for predicting stable amplitudes of vortex-induced vibrations. *Engineering* 3, 854-862.